X-ray, NMR, and Mutational Studies of the Catalytic Cycle of the GDP-Mannose Mannosyl Hydrolase Reaction[†,‡]

Sandra B. Gabelli,[§,||] Hugo F. Azurmendi,[||,⊥] Mario A. Bianchet,[§] L. Mario Amzel,*[,§] and Albert S. Mildvan*[,⊥]

Department of Biological Chemistry and Department of Biophysics and Biophysical Chemistry, The Johns Hopkins University School of Medicine, 725 North Wolfe Street, Baltimore, Maryland 21205-2185

Received June 21, 2006; Revised Manuscript Received August 1, 2006

ABSTRACT: GDP-mannose hydrolase catalyzes the hydrolysis with inversion of GDP-α-D-hexose to GDP and β-D-hexose by nucleophilic substitution by water at C1 of the sugar. Two new crystal structures (free enzyme and enzyme−substrate complex), NMR, and site-directed mutagenesis data, combined with the structure of the enzyme−product complex reported earlier, suggest a four-stage catalytic cycle. An important loop (L6, residues 119−125) contains a ligand to the essential Mg^{2+} (Gln-123), the catalytic base (His-124), and three anionic residues. This loop is not ordered in the X-ray structure of the free enzyme due to dynamic disorder, as indicated by the two-dimensional $^{1}H-^{15}N$ HMQC spectrum, which shows selective exchange broadening of the imidazole nitrogen resonances of His-124 ($k_{ex} = 6.6 \times 10^4\ s^{-1}$). The structure of the enzyme−Mg^{2+}−GDP-mannose substrate complex of the less active Y103F mutant shows loop L6 in an open conformation, while the structure of the enzyme−Mg^{2+}−GDP product complex showed loop L6 in a closed, "active" conformation. $^{1}H-^{15}N$ HMQC spectra show the imidazole Nε of His-124 to be unprotonated, appropriate for general base catalysis. Substituting Mg^{2+} with the more electrophilic metal ions Mn^{2+} or Co^{2+} decreases the pK_a in the pH versus k_{cat} rate profiles, showing that deprotonation of a metal-bound water is partially rate-limiting. The H124Q mutation, which decreases k_{cat} $10^{3.4}$-fold and largely abolishes its pH dependence, is rescued by the Y103F mutation, which increases k_{cat} 23-fold and restores its pH dependence. The structural basis of the rescue is the fact that the Y103F mutation shifts the conformational equilibrium to the open form moving loop L6 out of the active site, thus permitting direct access of the specific base hydroxide from the solvent. In the proposed dissociative transition state, which occurs in the closed, active conformation of the enzyme, the partial negative charge of the GDP leaving group is compensated by the Mg^{2+}, and by the closing of loop L2 that brings Arg-37 closer to the β-phosphate. The development of a positive charge at mannosyl C1, as the oxocarbenium-like transition state is approached, is compensated by closing the anionic loop, L6, onto the active site, further stabilizing the transition state.

GDP-mannose mannosyl hydrolases (GDPMHs)[1] catalyze the hydrolysis with inversion of GDP-α-D-hexoses to GDP and β-D-hexose (*1*−*4*).

$$\text{GDP-}\alpha\text{-D-hexose} + H_2O \rightarrow \text{GDP} + \beta\text{-D-hexose} + H^+ \quad (1)$$

The sequences of GDPMHs contain a modified version of the 23-residue signature sequence characteristic of Nudix hydrolases, a family of enzymes that catalyze the hydrolysis of compounds that include a nucleoside diphosphate (NDP) bound to an additional moiety (X) (*5*). Three characteristics distinguish the GDPMH subfamily from other Nudix enzymes. (i) Instead of the characteristic 23-residue signature sequence present in most of the other members of the family, $GX_5EX_7REUXEEXGU$, the sequence in GDPMH is $GX_5EX_7R(L/I)X_3ELGU$ (U is I, L, or V), which lacks two metal liganding glutamate residues. (ii) While most members of the Nudix family hydrolyze their substrates by associative nucleophilic substitution at phosphorus, GDPMH hydrolyzes GDP-mannose by a dissociative nucleophilic substitution at C1 of the sugar by hydroxide (*1*). (iii) While most Nudix enzymes use a glutamate as the catalytic base, GDPMH uses a histidine residue (*2*, *6*).

The three-dimensional structure of the *Escherichia coli* GDPMH in complex with GDP and Mg^{2+} (product complex) has been determined by X-ray diffraction methods to a resolution of 1.3 Å [PDB entry 1RYA (*7*)]. This complex crystallized with a Tris molecule from the mother liquor in the catalytic site. The Tris molecule is ∼3 Å from two of the oxygens of the β-phosphate of GDP, and its three OH

[†] This research was supported by National Institutes of Health Grants DK-028616 (to A.S.M.) and GM 066895 (to L.M.A.).

[‡] Coordinates of the structure of free GDPMH and of the Y103F−Mg^{2+}−GDP-mannose complex have been deposited in the Protein Data Bank (entries 2GT2 and 2GT4, respectively).

* To whom correspondence should be addressed. Telephone: (410) 955-2038. Fax: (410) 955-5759. E-mail: mildvan @jhmi.edu.

[§] Department of Biophysics and Biophysical Chemistry.

[||] These authors contributed equally to the work presented here.

[⊥] Department of Biological Chemistry.

[1] Abbreviations: AEBSF, 4-(2-aminoethyl)benzenesulfonyl fluoride hydrochloride; BCA, bicinchoninic acid; DTT, dithiothreitol; GDPMH, GDP-mannose mannosyl hydrolase; HMQC, heteronuclear multiple-quantum coherence; MOPS, 3-(*N*-morpholino)propanesulfonic acid; PCR, polymerase chain reaction; SDS−PAGE, sodium dodecyl sulfate−polyacrylamide gel electrophoresis; rmsd, root-mean-square distance.

10.1021/bi061239g CCC: $33.50
Published on Web 08/31/2006

groups participate in hydrogen bonds with residues His-88, Tyr-90, Ser-20, and Arg-37. Two of these residues (Arg-37 and His-88) were found by mutagenesis to be important for substrate recognition and catalysis (*1*). The position and interactions of the Tris molecule in the product complex were taken as to be indication that this molecule is occupying the position of the terminal sugar. Using the structure of product complex, a model was built of the ternary complex of the enzyme with Mg^{2+} and GDP-mannose (*7*). This model provided a rationale for the difference between GDPMH and other Nudix enzymes in the site of nucleophilic substitution: a six-residue deletion in a loop of GDPMH (loop 6) shifts the location of the general base, His-124, by approximately 6 Å to a position where it can catalyze the substitution at C1 of the mannose (*7*, *8*).

The structure of the GDPMH−Mg^{2+}−GDP complex (*7*) combined with mutational studies (*1*, *2*) shows extensive activation of the GDP leaving group by the essential Mg^{2+} and by Arg-37, Arg-52, Arg-65, and Tyr-103, suggesting a dissociative transition state, as generally found for glycosylating enzymes (*9*). A dissociative mechanism was further supported by the significant catalytic contribution of Asp-22, which is positioned well to stabilize an oxocarbenium ion, by His-88 and Tyr-90, which are positioned to distort the mannosyl group toward the transition state, and by the 16-fold lower k_{cat} found with GDP-2F-α-D-mannose as substrate, in which the electrophilic fluorine at C2 inhibits the formation of an oxocarbenium ion at C1 (*1*, *2*, *8*).

Despite extensive efforts, many questions about the mechanism of GDPMH remain unanswered. For example, in some Nudix enzymes, the active site is formed only when substrate and Mg^{2+} bind to the enzyme (*10*). This aspect of the mechanism is thought to contribute to enzyme specificity by requiring that Mg^{2+} and the correct substrate be present to bring the active site residues to their correct positions for catalysis. Is such a mechanism operative in GDPMH? Are there conformational changes involving loops that contain residues that are important for catalysis? To answer these questions, and to further examine the mechanism of GDPMH, we have determined the X-ray structures of the free enzyme and of the catalytically damaged Y103F mutant complexed with Mg^{2+} and the substrate GDP-α-D-mannose. The Y103F mutation was chosen because it had a significant catalytic effect, decreasing k_{cat} by 100-fold but not abolishing activity and permitting the retention of intact substrate during crystallization and data collection. We have complemented these structural studies with NMR experiments and with additional multiple mutations.

EXPERIMENTAL PROCEDURES

Materials. All reagents, enzymes, buffers, and solvents were obtained from Sigma Aldrich Chemical Co. (St. Louis, MO), unless otherwise noted. Enzyme-grade MOPS buffer and DTT were purchased from Fisher Scientific (Fair Lawn, NJ). Amicon Ultra (10 000 molecular weight cutoff) Millipore centrifugal filter devices were obtained from Fisher Scientific (Newark, DE). *E. coli* strain DH5α was purchased from Gibco BRL (Grand Island, NY). *E. coli* strain BL-21-(DE3) and QuikChange site-directed mutagenesis kits were purchased from Stratagene (La Jolla, CA). Plasmid DNA purification kits were purchased from Qiagen (Valencia, CA). $^{15}NH_4Cl$ (99%) was purchased from Cambridge Isotope Labs, Inc. (Andover, MA). Calf intestinal alkaline phosphatase was purchased from New England Biolabs Inc. (Beverly, MA). Tris-d_{11}-HCl was purchased from Isotec Inc. (Miamisburg, OH).

General Methods. Preparation of wild-type GDPMH (*3*) and the construction, characterization, and purification of the Y103F and D22A mutants, to ≥95% purity as judged by SDS−PAGE, are described elsewhere (*1*). The Y103F mutant gene was used as the template to generate the Y103F/H124Q double mutant, using the QuikChange site-directed mutagenesis kit (*1*). Similarly, the triple mutant Y103F/H124Q/E70Q was prepared using the Y103F/H124Q double mutant as a template. Coding and complementary noncoding mismatch primers, 33 residues in length, were used (*1*, *2*, *7*). The plasmids were subcloned into DH5α *E. coli* cells and purified using the Qiagen miniprep kit. For protein expression, the plasmids were cloned into BL-21(DE3) *E. coli* cells. The expressed plasmids were sequenced to verify the mutations and an otherwise unaltered DNA sequence. Uniformly ^{15}N-labeled wild-type GDPMH and the Y103F mutant were prepared as described previously (*1*).

Hydrolysis of GDP-mannose was quantitated by following the production of phosphate, upon treatment of the GDP product with calf intestinal alkaline phosphatase in a coupled enzyme assay, as described previously (*2*, *3*). To determine whether the site of bond cleavage on GDP-α-D-mannose remained unaltered in the reaction catalyzed by the Y103F/H124Q double mutant enzyme, a coupled assay for GDP formation was carried out using pyruvate kinase, *P*-enolpyruvate, L-lactate dehydrogenase, and NADPH (*11*). The concentration of GDPMH was determined by either UV absorption at 280 nm [using an ϵ_{280}^{native} of 72.8 mM^{-1} cm^{-1} at pH 6.5 in 20 mM phosphate buffer (*12*)] or the BCA assay using BSA as the standard (*13*). These methods agreed within 3%.

For kinetic measurements as a function of pH, Na^+-MES buffer was used for pH values between 5.8 and 7.0, Tris-HCl buffer was used in the pH range of 7.0−8.5, and Na^+-glycine buffer was used for pH values between 8.5 and 10.0. In studies of the effects of ionic strength on pK_a values, the indicated concentration of NaCl was added. All pH values were measured in parallel samples at the same temperature. Assays were carried out in a temperature-controlled bath for 15 min. Reaction mixtures (50 μL) contained 1−2 milliunits of GDPMH, 80 mM buffer, 20 mM $MgCl_2$, and 1 unit of calf intestinal alkaline phosphatase. The reactions were stopped by addition of 250 μL of a solution of 5 mM EDTA. For colorimetric determination of phosphate concentrations, 700 μL of Ames mix as described previously (*2*) was added. After color development (30 min at 37 °C), optical absorption was measured at 780 nm. An alternative and more sensitive colorimetric method was used in the pK_a studies of the Y103F mutant and the Y103F/H124Q double mutant in which the Ames mix was replaced with a malachite green mix (*14*). After allowing color development for 15 min at 37 °C, we measured optical absorption at 660 nm.

With the reduced activity of the Y103F/H124Q/E70Q triple mutant, the effect of pH on k_{cat} activated by Mg^{2+}, Mn^{2+}, or Co^{2+} was independently checked with an assay that did not require alkaline phosphatase but yielded the same results within experimental error. This assay used GDP-

mannose containing uniformly ^{14}C-labeled mannose, as described previously (*2*), permitting detection of the generation of free [^{14}C]mannose.

The pH dependence of k_{cat} was fit to the logarithmic form of eq 2, by nonlinear least-squares methods, as described previously (*15*)

$$k_{cat} = (k_{cat})^{max}/(1 + [H^+]/K_{H_2ES}) \quad (2)$$

to yield the pK_a ($-\log K_{H_2ES}$) of a group that must be deprotonated for catalytic activity.

Crystallization. Crystals of the free wild-type enzyme (in the absence of Mg^{2+}, substrate, or product) were grown at 18 °C by vapor diffusion in hanging drops with a protein: reservoir solution ratio of 1:1 (0.4 M potassium sodium tartrate). The crystals, which take more than 8 months to grow, belong to space group $P3_2$ with the following cell dimensions: $a = b = 48.8$ Å, and $c = 210.2$ Å. For data collection, crystals were flash-frozen in liquid nitrogen without a cryoprotectant. Crystals of the mutant Y103F GDPMH were grown at 18 °C by vapor diffusion using the sitting drop method. Y103F GDPMH, preincubated in a solution containing 5 mM GDP-mannose and 5 mM $MgCl_2$, was mixed in a 2:1 ratio with reservoir solution [20% PEG 4000, 100 mM Tris-HCl (pH 8.5), and 0.2 M $MgCl_2$]. Crystals belonging to space group *C*2 with the following cell dimensions appeared in 2 days: $a = 137.8$ Å, $b = 93.9$ Å, $c = 66.1$ Å, and $\beta = 91.2°$.

Structure Determination and Refinement. Diffraction data were collected on an ADSC Q315 detector using 1.1 Å synchrotron radiation at beam line X25 of the National Synchrotron Light Source at the Brookhaven National Laboratory (Upton, NY). All data were collected at 100 K. Intensity data were integrated, scaled, and reduced to structure factor amplitudes with the HKL2000 suite of programs (*16*). Data collection statistics are listed in Table 1. Molecular replacement was carried out with AMoRe (*17*) using the structure of the GDPMH−Mg^{2+}−GDP−Tris complex (PDB entry 1RYA) as a search model. Prior to refinement, 5% of the data was randomly flagged for cross validation. Restrained refinement of the models, minimizing a maximum-likelihood residual, was performed using REFMAC (*18*), monitoring the convergence of R_{cryst} and R_{free}. Manual building was carried out using O (*19*), and water molecules were placed automatically with Arp-WARP (*20*). The stereochemistry of the model was analyzed using PROCHECK (*21*). All structural superpositions were carried out with LSQMAN (*22*). Figures were drawn with MOLSCRIPT and PYMOL (*23*−*25*).

In the structure of the Y103F mutant of GDPMH, density was identified for GDP-mannose and Mg^{2+}. After refinement of the mutant enzyme, including the substrate and magnesium, $2F_o - F_c$ and $F_o - F_c$ density maps showed additional density continuous with the side chain of Asn-39. Attempts to interpret this density as a buffer component did not refine reliably, did not return well-defined density, and showed strong positive and negative peaks in the $F_o - F_c$ density maps. It was not until the density was interpreted as a mannose residue covalently linked to Nδ of Asn-39 that the refinement and the density maps improved significantly (Figure 8).

Table 1: Crystallographic Data Collection and Refinement Statistics

	free GDPMH	Y103F GDPMH
space group	$P3_2$	$C2$
cell dimensions	$a = b = 48.8$ Å, $c = 210.2$ Å	$a = 137.78$ Å, $b = 93.89$ Å, $c = 66.10$ Å, $\beta = 91.22°$
resolution range (Å)	50.00−2.00 (2.07−2.00)	50.0−2.30 (2.38−2.30)
R_{sym} (%) (last shell)	7.0 (20.6)	7.2 (40.6)
completeness (%) (last shell)	92.3 (63.8)	97.6 (99.9)
multiplicity (last shell)	4.1 (1.8)	3.0 (3.0)
$\langle I/\sigma(I)\rangle$	19.1	14.3
no. of observed reflections	143557	111382
refinement statistics		
R_{cryst}	0.20 (0.23)	0.19 (0.25)
R_{free}	0.25 (0.33)	0.23 (0.31)
no. of protein atoms	5288	4393
no. of waters	351	345
metal	−	3 Mg^{2+}
ligand	−	3 GDP-mannose
rms deviation		
bond lengths (Å)	0.008	0.010
bond angles (deg)	1.158	1.223
temperature factor (Å^2)		
protein	32.06	40.00
water	38.35	47.64
metal	−	28.00
ligands	−	40.69
Ramachandran distribution		
favored (%)	94.6	95.0
allowed (%)	5.4	5.0

Modeling of the Transition State. The structure of a partially dissociative transition state structure was modeled by docking an oxocarbenium form of GDP-α-D-mannose into the closed, "active", conformation of the enzyme found in the GDPMH−Mg^{2+}−GDP product complex using the position of the Tris molecule as a guide (*7*).

NMR Samples. The protein concentration of uniformly ^{15}N-labeled wild-type GDPMH and the Y103F mutant was 0.7 mM in 4 mM Tris-d_{11}-HCl buffer, 0.3 mM NaN_3, 21 mM NaCl, 10 mM DTT, 0.1 mg/mL AEBSF, and 10% D_2O. The indicated pH values were adjusted by addition of either 0.5 M HCl or 0.5 M NaOH solutions in microliter amounts. To minimize acid precipitation of wild-type GDPMH and the Y103F mutant, 1.0 M Na^+-MES buffer at pH 5.0 was used to adjust the pH to low values. NMR spectra were obtained on a Varian INOVA 600 MHz NMR spectrometer equipped with a triple-resonance cryoprobe with *Z*-gradient capacity.

Standard $^1H-^{15}N$ HSQC spectra were collected at 30 °C and pH 7.5 to observe amide backbone resonances as described previously (*1*, *2*). Mutant enzymes were examined for structural changes by comparing their two-dimensional $^1H-^{15}N$ HSQC spectra with that of the wild-type enzyme. The number of resonances with changes in chemical shifts of ≥ 0.5 ppm in the ^{15}N dimension and/or ≥ 0.05 ppm in the proton dimension were counted and are listed in Table S1 of the Supporting Information. Although the backbone ^{15}N and NH resonances of this homodimer have not been assigned, changes in their chemical shifts provide a sensitive phenomenological measure of structural changes (*1*, *2*). To observe the signals from the coupled ^{15}N and ^1HC in the imidazole ring of the histidine residues, a long-range $^1H-^{15}N$ HMQC sequence was used (*26*), modified to include selective ^{15}N excitation pulses to minimize excitation of

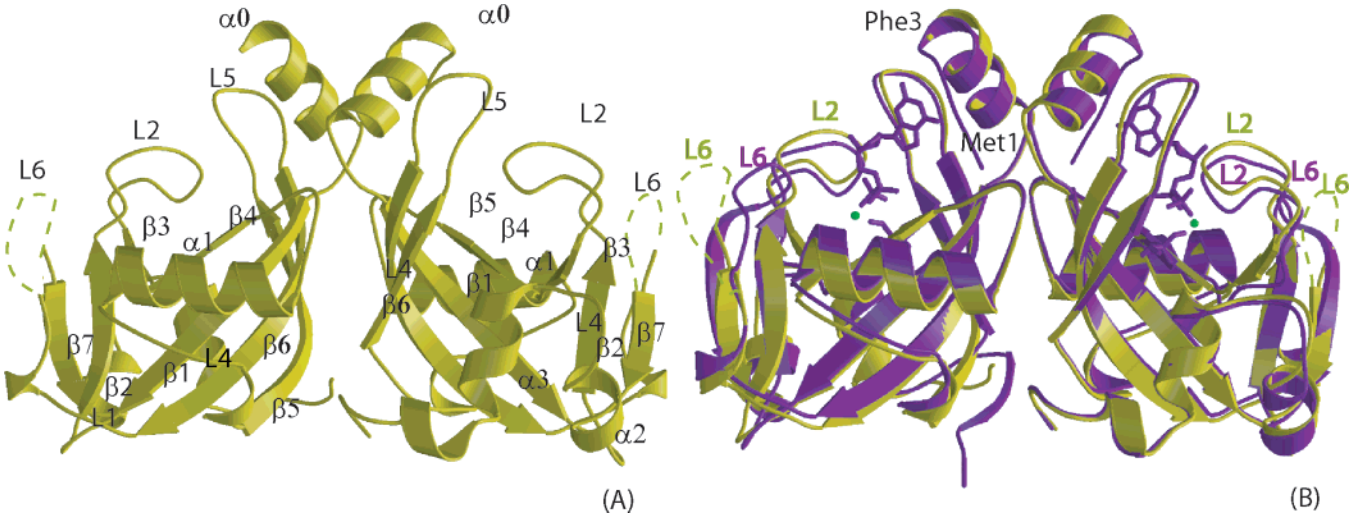

FIGURE 1: Overall structure of free wild-type GDPMH. (A) GDPMH is a dimer of 160 residues per monomer. Residues 119−125 (loop L6) are not seen in the electron density due to disorder. Disordered residues include Q123 (metal ligand) and H124 (catalytic base). (B) Overlap of the structures of the free wild-type GDPMH (gold) and the wild-type GDPMH−Mg^{2+}−GDP−Tris complex (purple).

backbone amide nitrogens, with spectral widths of 6600 Hz centered at 210 ppm in the ^{15}N dimension and spectral widths of 8000 Hz centered at 4.73 ppm in the proton dimension. The data were processed using NMRPipe (*27*) and analyzed with Sparky (*28*) or NMRDraw (*27*).

To determine the pK_a values of the titratable histidines, the HMQC spectra were collected with only eight FIDs (real and imaginary) in the ^{15}N dimension (*2*). This approach allows faster and more accurate measurements of the chemical shifts directly from the one-dimensional ^1H spectra in cases of overlapping peaks, because the evolution of overlapping signals in the indirect dimension can be separated in at least one of the eight spectra due to differences in the phases of the individual signals. Fourier transformation of the individual FIDs in the ^1H dimension showed well-resolved resonances with no interfering signals from the backbone NH groups.

The pH titration data were fit to eq 3

$$\Delta\delta = [\delta_1 + \delta_2(10^{pH-pK_a})^n]/[(10^{pH-pK_a})^n + 1] \quad (3)$$

to yield the low-pH (δ_1) and high-pH (δ_2) limits for the chemical shift change during the titration, the Hill coefficient (n), and the pK_a, as described previously (*2*).

RESULTS AND DISCUSSION

Overall Structure of Free GDPMH. The free wild-type enzyme crystallizes in space group $P3_2$ with two dimers in the asymmetric unit (dimer 1, monomers A and B, Figure 1A; dimer 2, monomers C and D). The dimer is similar (rmsd = 0.94 Å) to that observed in the structure of the GDPMH−Mg^{2+}−GDP−Tris complex (product complex) (*7*).

Each monomer contains seven β-strands and four helices connected by loops. Residues in loop L6 (A119−125, B120−125, C122−125, D120−124) and some of the N-terminal residues (A1−2, B1−4, C1, D1−3) are not observed in the electron density map. The N-terminal helix and two of the strands are involved in dimer contacts. In all monomers, the active site cavity is populated with 13 water molecules.

Comparison of the Structures of Free GDPMH and the Product Complex. In the structure of the free enzyme, Phe-3 in the monomers in which it is ordered and residues 4−9 in all monomers adopt a conformation that is different from that observed in the structure of the product complex, in which they stack on both sides of the guanine base. This observation suggests that residues 3−9 form the binding site for the guanine base of GDP, but only when substrate or product is bound to the enzyme. The main chain of loop L2 (residues 37−43), which contains Arg-37 and is involved in phosphate recognition, is 1.2 Å farther from the active site in the free enzyme than in the product complex (Figure 1B). The position of Arg-37 is closer to its position in the Y103F mutant (see below) than to that in the product complex. Phe-47, which interacts with a Tris molecule in the product complex, adopts a different rotamer in the free enzyme.

As mentioned above, loop L6 (residues 119−125), which contains His-124, the catalytic base, and Gln-123, a metal ligand, is not observed in the electron density map of the free enzyme (Figure 1). This observation correlates with the broadening of the imidazole ^{15}N resonance of His-124 in the $^1H-^{15}N$ HMQC spectrum of free GDPMH (see below). In the free enzyme, in addition to the disorder of loop L6, strand β2 (residues 34−36) together with its hydrogen-bonded partner, strand β7 (residues 126−128), is shifted with respect to its position in the product complex. These changes suggest a concerted conformational change taking place upon substrate−product binding (Figure 1).

Tautomeric Forms of the Histidine Residues of GDPMH and Its Mutants in the Product Complex. The tautomeric structures of the neutral histidine side chains were determined by heteronuclear NMR, making use of the fact that $^{15}N\epsilon$ of the imidazole ring is strongly coupled to both $^1HC\delta$ and $^1HC\epsilon$, while $^{15}N\delta$ is strongly coupled only to $^1HC\epsilon$ (*2*, *26*, *29*). Figure 2A shows a two-dimensional $^1H-^{15}N$ HMQC spectrum of the imidazole region of wild-type GDPMH in the presence of Mg^{2+}, GDP, and Tris as in the X-ray structure of the product complex (*7*), at pH 8.3 where all of the histidines are in their neutral forms. The sequence-specific ^{15}N and ^1HC assignments were previously made by comparing the spectra of the individual histidine mutants of free GDPMH with that of the wild-type enzyme (*2*). As shown

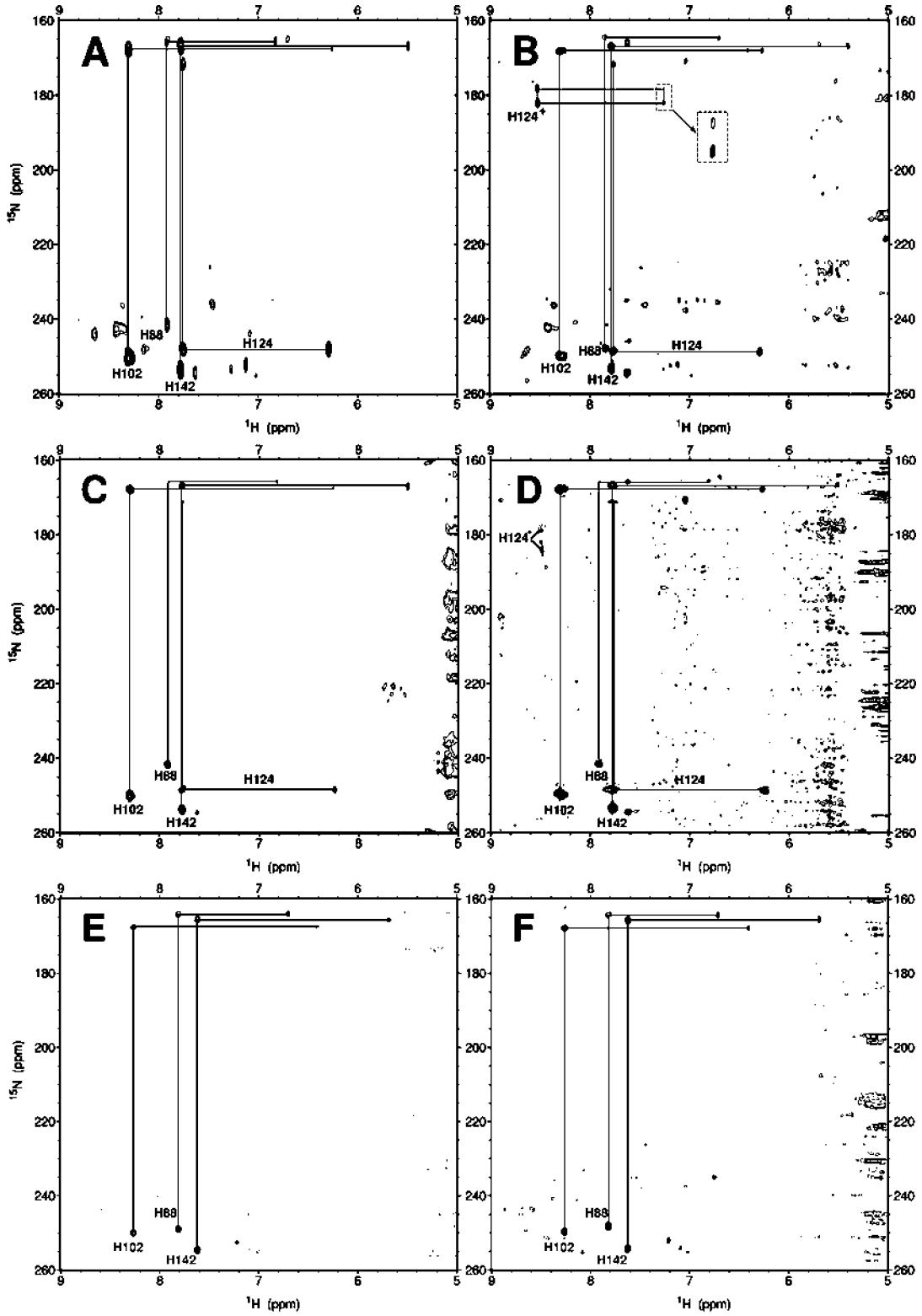

FIGURE 2: Two-dimensional $^{1}H-^{15}N$ HMQC spectra of the imidazole region of the ternary enzyme$-Mg^{2+}-$GDP complexes of wild-type GDPMH and the Y103F and Y103F/H124Q mutants at 30 °C. Assignments were made by individual site-directed mutations of His to Gln (*2*). (A) GDPMH$-Mg^{2+}-$GDP complex at pH 8.3. Note the Γ-arrangement of cross-peaks of His-88, His-102, and His-142, indicating the NϵH tautomers of their neutral forms, and the L-arrangement of cross-peaks of His-124, indicating the NδH tautomer of its neutral form. (B) GDPMH$-Mg^{2+}-$GDP complex at pH 6.1. Note the appearance of four cross-peaks from the cationic form of His-124 and the decreased intensity of the signals of the neutral form of His-124. The inset shows a 2-fold enlargement of both the ^{1}H and ^{15}N scales at a 1.4-fold lower contour level. (C) Y103F$-Mg^{2+}-$GDP complex at pH 8.3. (D) Y103F$-Mg^{2+}-$GDP complex at pH 6.5. (E) Y103F/H124Q$-Mg^{2+}-$GDP complex at pH 8.3. (F) Y103F/H124Q$-Mg^{2+}-$GDP complex at pH 6.5. The following components were present: wild-type or mutant GDPMH (1.0 mM in subunits), 1.3 mM $MgCl_2$, 1.3 mM GDP, 4.0 mM Tris-d_{11}-HCl, 21 mM NaCl, 10 mM DTT, 0.3 mM NaN_3, 0.1 mg/mL AEBSF, and 10% D_2O. To avoid acid precipitation of the protein, the pH of sample B was lowered to 6.1 and the pHs of samples D and F were lowered to 6.5 by adding microliter quantities of 1.0 M Na^{+}-MES (pH 5.0).

Table 2: Imidazole Resonances and pK_a Values of His-124 of GDPMH from NMR Experiments at 30 °C[a]

enzyme	pH	δ (ppm) ^{1}HCδ	^{1}HCϵ	^{15}Nδ	^{15}Nϵ	pK_a	n
WT	6.1	7.30	8.51	183.7	178.58	7.20 ± 0.07[b]	0.81 ± 0.20[b]
	8.3	—[c]	7.84	205	205		
WT−Mg^{2+}−GDP	6.1 (cationic)	7.26	8.52	178.1	182.1	7.31 ± 0.05	1.10 ± 0.12
	6.1 (neutral)	6.29	7.77	171.6	248.7		
	8.3	6.29	7.76	171.8	248.1		
Y103F	6.5	7.21	8.43	180.4	186.5	7.25 ± 0.05	1.06 ± 0.11
	8.3	—[c]	7.85	—[c]	—[c]		
Y103F−Mg^{2+}−GDP	6.5 (cationic)	—[c]	8.49	178.5	183.9	7.34 ± 0.06	1.02 ± 0.12
	6.5 (neutral)	6.24	7.78	171.2	248.6		
	8.3	6.24	7.77	171.2	248.4		

[a] Note that the NδH tautomer of the neutral form is found. The errors in δ were ±0.01 ppm in the proton dimension and ±0.1 to ±0.5 ppm in the ^{15}N dimension. [b] From ref *2*. [c] Resonances were not resolved.

in Figure 2A, His-88, His-102, and His-142 show strong couplings of both their HCδ and HCϵ resonances to upfield Nϵ signals, forming a Γ-pattern, indicating Nϵ to be protonated and Nδ to be unprotonated in the neutral forms of these residues. In contrast, His-124 shows strong couplings of both HCδ and HCϵ to a downfield Nϵ, forming an L-pattern, indicating Nϵ to be unprotonated and Nδ to be protonated. The NMR data established that Nϵ of His-124 which is 3.8 Å from a Mg^{2+}-bound water in the X-ray structure (*7*) is unprotonated, consistent with the functioning of His-124 as the general base. At pH 6.1 (Figure 2B), four cross-peaks, all upfield in the ^{15}N dimension, form a rectangular array reflecting the cationic form of His-124.

The imidazole HMQC spectrum of the ternary Y103F−Mg^{2+}−GDP complex of the mutant at pH 8.3 is very similar to that of the wild-type enzyme (Figure 2C). At pH 6.5 (Figure 2D), the signal of the neutral form of His-124 is attenuated and that of the protonated form is detectable, although the upfield signals from CδH were not resolved. Table 2 summarizes the imidazole ^{1}H and ^{15}N chemical shifts and pK_a values of His-124 in both wild-type GDPMH and in the Y103F mutant under various conditions. The imidazole chemical shifts of the other three histidines of wild-type GDPMH and of the Y103F mutant are summarized in Tables S2 and S3, respectively, of the Supporting Information. The imidazole HMQC spectra of the ternary Y103F/H124Q−Mg^{2+}−GDP complex at pH 8.3 (Figure 2E) and at pH 6.5 (Figure 2F) are very similar to those of the wild type and the Y103F mutant, differing only in the absence of resonances assigned to His-124 (Table S4).

^{1}H−^{15}N Imidazole HMQC Spectra of Free Wild-Type GDPMH and the Free Y103F Mutant. In the absence of Mg^{2+} and GDP, the imidazole resonances of His-124 in free, wild-type GDPMH at pH 8.3 show a well-resolved ^{1}HCϵ signal in the proton dimension at 7.84 ppm, but no CδH resonance, likely due to exchange broadening (Figure 3). Consistent with exchange broadening, a single, broad resonance centered at 205 ± 5 ppm, with a line width of 2700 Hz, is seen in the ^{15}N dimension. This chemical shift averaging likely results from fast proton exchange at both the Nδ and Nϵ positions of His-124 at a rate exceeding their chemical shift difference in the ^{15}N dimension [76.3 ppm (Table 2)]. Analysis of the line shape (*30*) yields an exchange rate ($1/\tau_{ex}$) of 6.6×10^4 s^{-1} at 30 °C. Such fast exchange in free GDPMH suggests that the absence of significant density for loop L6 (residues 119−125) in the X-ray structure is a result of dynamic rather than static disorder. This exchange rate is greatly slowed in the enzyme−Mg^{2+}−GDP complex, where His-124 forms a well-resolved NδH tautomer (Figure 2A).

Unlike wild-type GDPMH, the free Y103F mutant shows no signals from His-124 in the ^{15}N dimension at pH 8.3, although the ^{1}HCϵ signal was readily detected in the proton dimension at 7.85 ppm in the first slice of the HMQC experiment (Table 2). Hence, extensive exchange broadening of the ^{15}N signals likely occurs, consistent with a rapidly changing environment for neutral His-124 in the Y103F mutant (not shown). Lowering the pH of the Y103F mutant to 6.5 resulted in the appearance of the upfield rectangular array of signals of the cationic form of His-124, like those found with the wild-type enzyme (*2*) (Table 2), indicating a decreased rate of exchange of the fully protonated form of His-124.

pK_a Values of His-124 from NMR Titrations and Comparison with Kinetics. One-dimensional proton slices of the ^{1}H−^{15}N HMQC spectra of wild-type GDPMH complexed with Mg^{2+} and GDP were collected as a function of pH between pH 6.0 and 9.6 at 30 °C (Figure 4B). Fitting the data to eq 3 yielded a pK_a of 7.31 ± 0.05 for His-124 in the ternary GDPMH−Mg^{2+}−GDP complex with a Hill coefficient (n) of 1.10 ± 0.12 (Table 2). NMR titration of free wild-type GDPMH yielded essentially the same pK_a for His-124 of 7.20 ± 0.07 (Hill coefficient of 0.81 ± 0.20) (Table 2), while those of the other histidines are below 5.5 (*2*). NMR titration of the Y103F mutant complexed with Mg^{2+} and GDP, as a function of pH (Figure 4A and Table 3), yielded a pK_a of 7.34 ± 0.06 for His-124 with a Hill coefficient of 1.02 ± 0.12. NMR titration of the free Y103F mutant yielded essentially the same pK_a for His-124 of 7.25 ± 0.05 and a Hill coefficient of 1.06 ± 0.11 (Figure 4A and Table 2) (*2*).

The pK_a values of His-124 determined by NMR (7.20−7.34) (Table 2) differ from the pK_a values determined kinetically (from pH vs k_{cat}), which are 6.70 ± 0.06 for wild-type GDPMH (*2*) and 6.56 ± 0.06 for the Y103F mutant (Table 3). Moreover, even when His-124 is absent, as in the H124Q/Y103F double mutant, and in the H124Q/Y103F/E70Q triple mutant, the kinetically determined pK_a values (at 37 °C) are 7.49 ± 0.03 and 7.33 ± 0.08 (Table 3). These observations raise the question of the origin of the kinetically determined pK_a values.

Tests for General Base Catalysis in the Y103F, Y103F/H124Q, and Y103F/H124Q/E70Q Mutants. An unknown

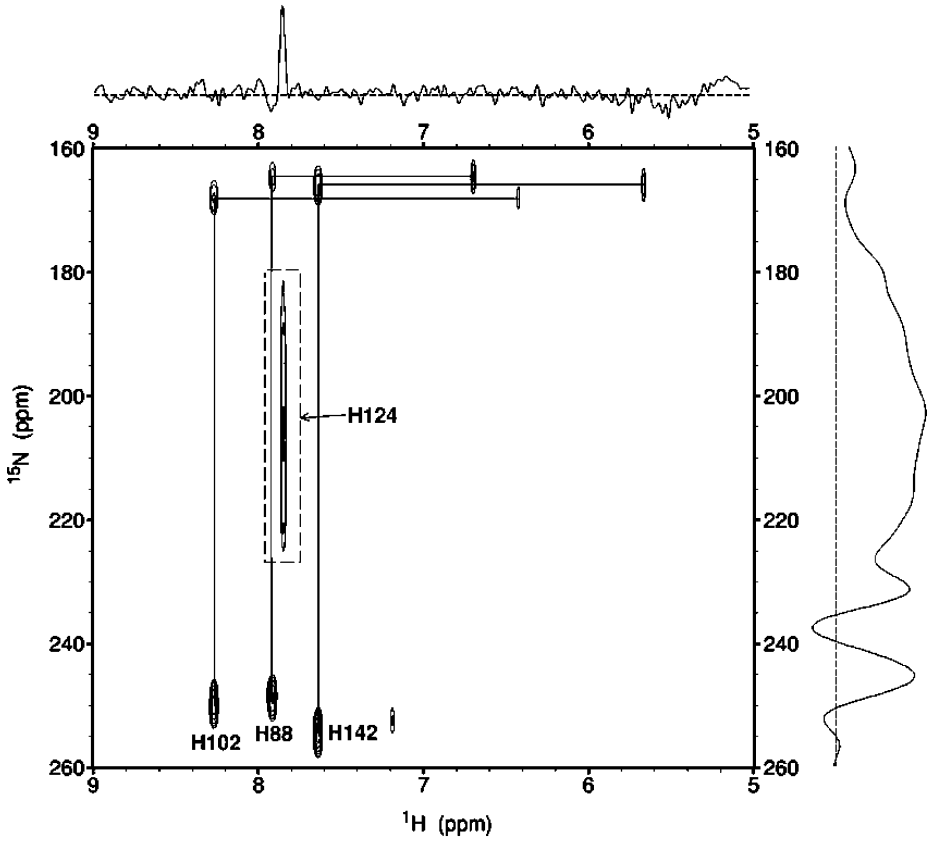

FIGURE 3: Two-dimensional $^{1}H-^{15}N$ HMQC spectrum of the imidazole region of free, wild-type GDPMH at 30 °C and pH 8.3, under conditions otherwise identical to those described in the legend of Figure 2A. The one-dimensional slice in the ^{1}H dimension is taken at $\delta(^{15}N) = 202$ ppm. The one-dimensional slice in the ^{15}N dimension is taken at $\delta(^{1}H) = 7.84$ ppm.

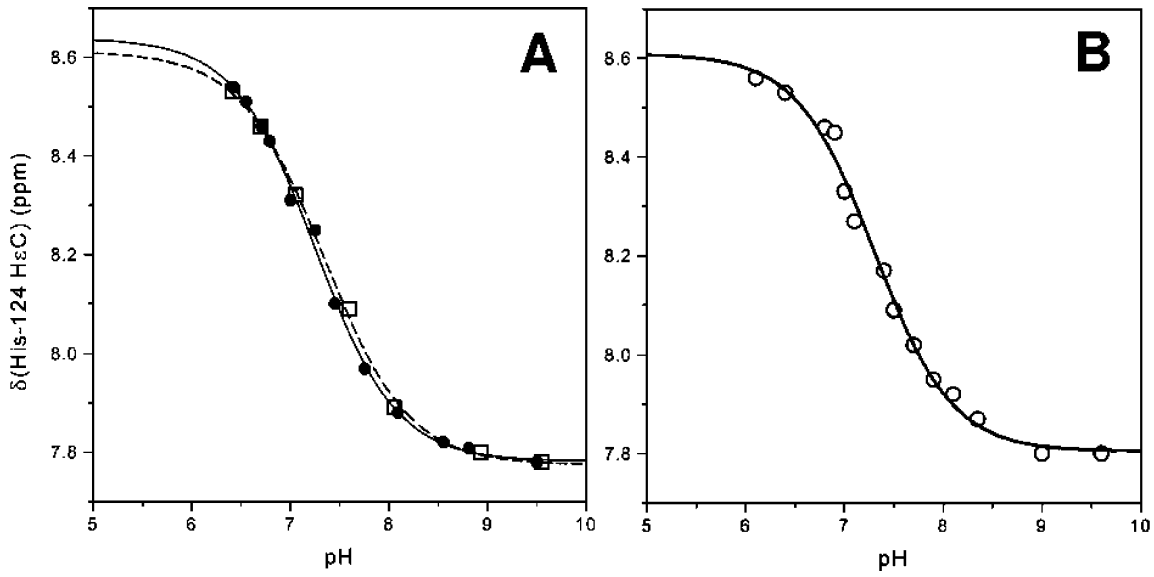

FIGURE 4: Heteronuclear NMR titrations as a function of pH of His-124 of the wild type and the Y103F mutant of GDPMH at 30 °C. (A) pH titration by heteronuclear NMR of His-124 in the free Y103F mutant (●) and complexed with Mg^{2+} and GDP (□). The solid and dashed curves correspond to theoretical fits of the data to eq 3 for the free and complexed forms of Y103F, respectively, yielding pK_a values of 7.25 ± 0.05 and 7.34 ± 0.06, respectively, with Hill coefficients of 1.06 ± 0.11 and 1.02 ± 0.12, respectively. (B) pH titration of His-124 in the GDPMH−Mg^{2+}−GDP complex of the wild-type enzyme (○). The solid curve corresponds to a theoretical fit of the data to eq 3, yielding a pK_a of 7.31 ± 0.05 and a Hill coefficient of 1.10 ± 0.11.

group other than His-124, with a kinetically determined pK_a of 6.56 in the Y103F single mutant, 7.49 in the Y103F/H124Q double mutant, and 7.33 in the Y103F/H124Q/E70Q triple mutant and probably also in wild-type GDPMH (pK_a = 6.70), is responsible for the ascending limb of the k_{cat} versus pH profile. In the Y103F mutant, the pK_a of this base increases with an increase in ionic strength and decreases with an increase in temperature, with a $\Delta H^{deprotonation}$ of 15.0 ± 1.4 kcal/mol, as might be expected for a nitrogen base (*31*) or a very unusual carboxyl group (Figure 5). However,

Table 3: Effects of Mutations on Kinetic Parameters of GDPMH with Mg^{2+} Activation and GDP-α-D-Mannose as Substrate at pH 9.3 and 37 °C

enzyme	k_{cat} (s^{-1})	K_m (mM)	fold decrease in k_{cat}	fold change in K_m	pK_a affecting k_{cat}
WT[a]	0.33	0.67	1.0	1.0	6.70 ± 0.06
Y103F[a]	0.0032	4.6	$10^{2.0}$	6.9	6.56 ± 0.06
R37Q[a]	0.0138	5.7	$10^{1.4}$	8.5	nd[b]
H124Q[c]	0.00031	1.5	$10^{3.4}$	4.7	none[d]
E70Q[c]	0.0049	3.2	$10^{2.2}$	10.0	6.87 ± 0.25
H124E[a]	0.0020	2.7	$10^{2.2}$	6.0	7.66 ± 0.07
D22A[a]	0.0027	3.0	$10^{2.1}$	4.5	7.20 ± 0.07
R37Q/Y103F[a]	0.00175	3.0	$10^{2.3}$	4.5	nd[b]
H124Q/Y103F	0.0070	2.3	$10^{1.7}$	3.4	7.49 ± 0.03
H124Q/Y103F/E70Q	0.0014	0.68	$10^{2.4}$	1.0	7.33 ± 0.08

[a] From ref *1*. [b] Not done. [c] From ref *2* in which the k_{cat} of WT was 0.71 s^{-1} and the K_m was 0.32 mM. [d] k_{cat} increased with pH in proportion to $[OH^-]^{0.17}$ (*2*).

no nitrogenous or free carboxylate groups are seen within 6 Å of the Mg^{2+}-bound water nucleophile (W2) at the active site of the Y103F mutant (see below), and none, other than His-124, is seen in the wild-type enzyme (*7*).

Asp-22 approaches another water molecule, W10 (3.4 Å), which is in contact with C1 of the modeled mannose in wild-type GDPMH (*7*) and is similarly positioned in the Y103F mutant. Despite this location, Asp-22 is unlikely to function as a general base because the D22A single mutant exhibits an only $10^{2.0}$-fold lower k_{cat} than wild-type GDPMH (*1*) and a normal pH−rate profile with a kinetically detected pK_a of 7.20 ± 0.07 (Table 3).

Glu-70 provides a carboxylate ligand to Mg^{2+}, and the carboxylate oxygen of Glu-70 that is not coordinated by the metal is sufficiently close to accept a hydrogen bond from the adjacent nucleophilic water ligand of Mg^{2+}, W2 (2.7 and 3.2 Å in subunits A and B of the product complex, respectively). To deprotonate this water molecule, and thereby to function as the general base, Glu-70 could transiently dissociate from the Mg^{2+} as the transition state is approached, in a process that requires heat. This possibility was tested by preparing the triple mutant, Y103F/H124Q/E70Q. Adding the E70Q mutation [which alone decreased k_{cat} 67-fold and increased K_m 4.8-fold (*2*)] to the Y103F/H124Q double mutant further decreased k_{cat} by only 5.0-fold (to 0.0014 s^{-1}) and decreased K_m 3.4-fold (to 0.68 mM) (Table 3). Moreover, the effect of pH on k_{cat} yielded a pK_a value of 7.33 ± 0.08, which was very similar to that found with the double mutant Y103F/H124Q (7.49 ± 0.03) (Table 3). These observations rule out general base catalysis by Glu-70.

Tests for Catalysis by Small Exogenous Bases. Varying the concentrations of Tris-HCl and of glycine buffers from 1.0 to 50 mM in the standard assay of the Y103F/H124Q double mutant at pH 9.3, and at 37 °C, or adding 4-methylimidazole at concentrations ranging from 1.0 to 300 mM did not increase k_{cat}, providing no evidence for catalysis by external nitrogenous bases.

Effect of Changing the Metal Activator on the pK_a in k_{cat}. By exclusion, the metal-bound water molecule, W2, could be responsible for the kinetically detected pK_a of 6.70 ± 0.06 in wild-type GDPMH, 6.56 ± 0.06 in the Y103F single mutant, 7.49 ± 0.03 in the Y103F/H124Q double mutant, and 7.33 ± 0.08 in the Y103F/H124Q/E70Q triple mutant (Table 3). To test for this, initially using wild-type GDPMH,

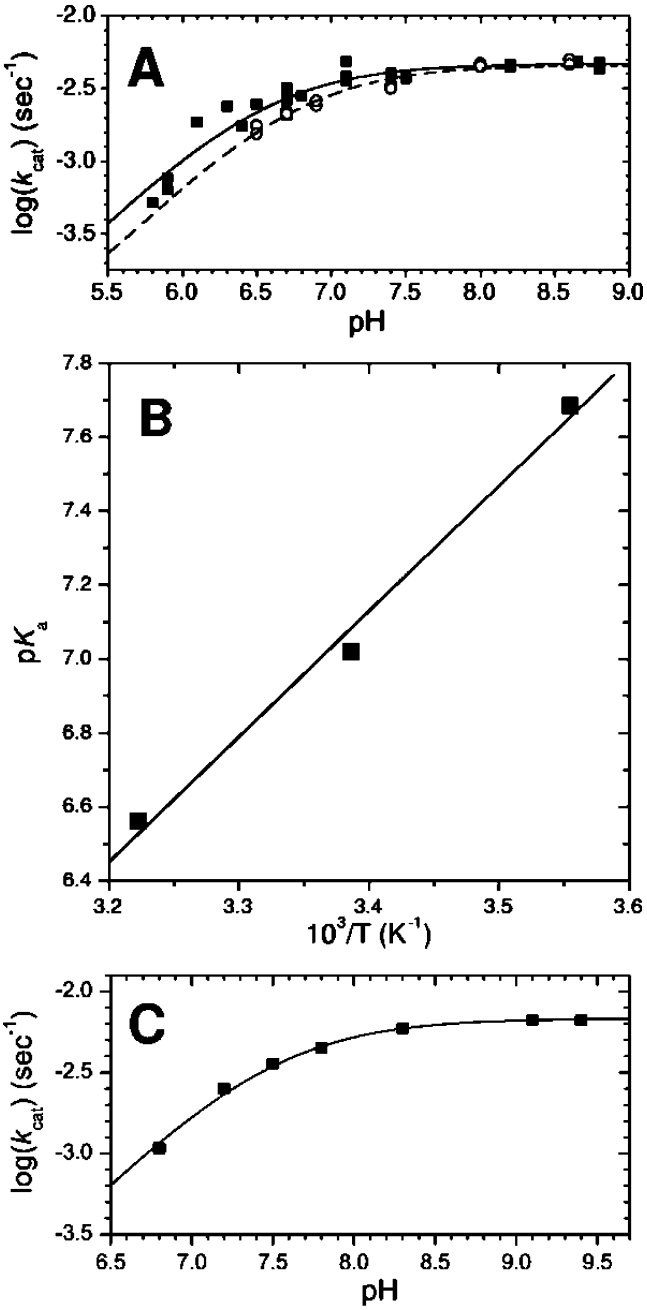

FIGURE 5: Effect of ionic strength and temperature on the single deprotonation observed in the plot of pH vs log(k_{cat}) of the Y103F mutant and pH titration of the Y103F/H124Q double mutant. (A) pH dependence of log(k_{cat}) of the Y103F mutant at 0.0 (■) and 0.3 M NaCl (○) at 37 °C. The curves are theoretical fits of the data to eq 2 which yield the pK_a values of 6.56 ± 0.06 and 6.78 ± 0.05, respectively. (B) van't Hoff plot showing the effect of temperature on the kinetically determined pK_a from pH vs k_{cat} studies. The pK_a of the Y103F mutant was measured at 8, 22, and 37 °C. The slope of the line equals $\Delta H^{ionization}/(2.3R)$, which leads to a $\Delta H^{ionization}$ of 15.0 ± 1.4 kcal/mol. (C) pH dependence of log(k_{cat}) of the Y103F/H124Q double mutant which yields a pK_a of 7.49 ± 0.03.

the activator Mg^{2+} was replaced with the more electrophilic divalent cations, Mn^{2+} and Co^{2+} , which also activate the enzyme.[2] The relative electrophilicities of metal ions correlate inversely with the pK_a values of their coordinated water

[2] With wild-type GDPMH, at the optimum pH, the relative $(k_{cat})^{max}$ values with Mg^{2+}, Mn^{2+}, and Co^{2+} are 100, 82, and 3.2%, respectively. With the Y103F/H124Q/E70Q triple mutant, the relative $(k_{cat})^{max}$ values are 100, 18, and 35%, respectively.

Table 4: Effect of Changing the Divalent Cation on the pK_a of a Water Ligand and the k_{cat} of the Y103F/H124Q/E70Q Triple Mutant and Wild-Type GDPMH

metal activator	pK_a of $M^{2+}-OH_2$[a]	ΔpK_a	Y103F/H124Q/E70Q mutant		wild type	
			pK_a in k_{cat}	ΔpK_a	pK_a in k_{cat}	ΔpK_a
Mg^{2+}	11.5−12.5	−	7.33 ± 0.08	−	6.80 ± 0.06	−
Mn^{2+}	10.5−10.7	0.8−2.0	6.45 ± 0.09	0.9	6.02 ± 0.04	0.8
Co^{2+}	8.9−9.6	1.9−3.6	≤5.6	≥ 1.7	5.64 ± 0.13	1.2

[a] From refs *32*−*34*.

ligands (*32*−*34*). In a fully aqueous environment, the pK_a values for water ligands of Mg^{2+}, Mn^{2+}, and Co^{2+} are 12.0 ± 0.5, 10.6 ± 0.1, and 9.2 ± 0.4, respectively (*32*−*34*) (Table 4). In agreement with the electrophilicities of these divalent cations which increase in the order $Mg^{2+} < Mn^{2+} < Co^{2+}$, with the wild-type GDPMH, replacing Mg^{2+} with Mn^{2+} decreased the kinetically determined pK_a in k_{cat} as a function of pH from the value of 6.80 ± 0.06 by 0.8 unit to a value of 6.02 ± 0.04. Activation by the more electrophilic Co^{2+} further decreased the pK_a in k_{cat} to 5.64 ± 0.13, a value 1.2 units below that found with Mg^{2+} (Table 4). While the absolute values of these kinetically determined pK_a values are far lower than those found in a fully aqueous environment, their order ($Co^{2+} < Mn^{2+} < Mg^{2+}$) and their differences (ΔpK_a values) (Table 4)[2] are consistent with the deprotonation of a metal-bound water ligand (*34*). The low pK_a values of metal-bound water W2 can be partially explained by the interaction with His-124 which is largely protonated at pH 6.7 (pK_a = 7.2−7.3).

With the Y103F/H124Q/E70Q triple mutant, very similar effects of changing the divalent cation activator on the pK_a of k_{cat} as a function of pH were observed. The pK_a values decreased with an increase in electrophilicity, in the same order as with the wild type, and showed similar ΔpK_a values (Table 4). These data, and previous observations that the pK_a in k_{cat} increased to 7.66 (from 6.70) in the H124E mutant (*1*), that the pK_a was abolished in the H124Q mutant and was replaced by a weak dependence of k_{cat} on $[OH^-]^{0.17}$ (*2*), suggest that deprotonation of metal-bound water W2 is responsible for the kinetically determined pK_a in k_{cat} in all cases, which ranges from 6.6 to 7.7 (Table 3). His-124, with its well-matched pK_a of 7.20−7.34 (Figure 4 and Table 3), when properly positioned, aids in this deprotonation by lowering the pK_a of the water molecule, contributing a factor of $10^{3.4}$ to catalysis (*2*). In the H124Q mutant, the altered residue Gln-124 may occlude access to metal-bound water W2 by external hydroxide, decreasing the reaction rate and the kinetic order in OH^- concentration to 0.17 (*2*). Another important role of the divalent cation in catalysis, in addition to decreasing the pK_a of W2, is to promote the departure of the GDP-leaving group. Since the k_{cat} of GDPMH does not correlate with the electrophilicity of the metal activator,[2] other factors including the detailed geometry of the active complex contribute to the values of k_{cat}.

The $^1H-^{15}N$ HSQC spectrum of the Y103F mutant exhibited seven backbone resonances of 172 that shifted in the ^1H dimension and one that shifted in the ^{15}N dimension in comparison with those of the wild-type enzyme (Table S1). The Y103F/H124Q/E70Q triple mutant exhibited 13 backbone resonance shifts in the ^1H dimension and five in the ^{15}N dimension, indicating largely intact backbone structures.

X-ray Structure of the Y103F Mutant of GDPMH in Complex with Mg^{2+} and GDP-α-D-Mannose. Determination of the structure of the GDPMH−Mg^{2+}−GDP-mannose complex (substrate complex) was carried out using the Y103F mutant, which has a k_{cat} 2 orders of magnitude lower than that of the wild-type enzyme (*1*, *7*) (Table 3). This reduction in k_{cat} allows the substrate and Mg^{2+} to remain in the active site of the enzyme as the crystals are formed, without noticeable hydrolysis during the crystallization period. The structure has three monomers in the asymmetric unit, two of which form a dimer similar to that observed previously (*7*). The third molecule uses the crystallographic two fold to form an equivalent dimer.

All monomers contain GDP-mannose and Mg^{2+} in their catalytic site. In all monomers, the hydroxyl groups of the mannose of the substrate form hydrogen bonds with the side chains of Arg-37 (to OH6), His-88 (to OH4), Tyr-90 (to OH4), Ser-20 (to OH3), and Asp-22 (to OH2 and OH3) (Figure 6). On the basis of this structure, it can be inferred that GDP-α-D-glucose, also a substrate of GDPMH, will make the same H-bonds with the exception of the epimeric OH at C2 of glucose, which is predicted to bind to Oγ of Ser-20. However, the K_m of GDP-α-D-glucose is 2.9-fold greater than that of GDP-α-D-mannose with wild-type GDPMH (*1*). Phe-103 (Tyr-103 in the wild type) stacks onto the hydrophobic face of the sugar (Figure 6). The interactions predicted by the model of the substrate complex based on the structure of the product complex are in good agreement with the interactions observed in the actual substrate complex, with the exception that in the substrate complex the Gln-123 carboxamide ligand to the Mg^{2+} ion is replaced with a water ligand.

The enzyme−substrate interactions are very similar in the three monomers. The interactions observed in monomer B will be described more extensively as an example of the details of the atoms involved, and their distances (Figure 6). Two water molecules are within hydrogen bonding distance of the pyranose ring oxygen of the mannose. The mannosyl O4H is the donor of a hydrogen bond to unprotonated Nδ of His-88 (assigned as unprotonated by NMR; distance 2.70 Å) and accepts a hydrogen bond from Tyr-90 (2.56 Å). Accordingly, the H88Q mutation increases the K_m of GDP-α-D-mannose 4.4-fold (*2*). The mannosyl O3H receives a hydrogen bond from OG1 of Ser-20 (2.80 Å) and donates a hydrogen bond to OD1 of Asp-22 (2.75 Å). The mannosyl O2H is also the donor of a hydrogen bond to OD1 of Asp-22 (2.61 Å) and is a short distance from W10 (2.98 Å), which is 3.5 Å from the reaction center C1 of the mannosyl group. Accordingly, the K_m of GDP-α-D-mannose increased by 4.5-fold in the D22A mutant and by 8.7-fold in the D22N mutant (*1*). C6 of the mannose stacks against Phe-47, which shifts from its position observed in the product complex to maximize apolar interactions.

Comparison of the Structures of the Substrate and Product Complexes. The most dramatic structural difference between the product complex (with the wild-type enzyme) and the substrate complex (with the Y103F mutant) occurs in loop L6, which contains the metal ligand Gln-123, the general base His-124, and three anionic residues, Asp-121, Glu-122, and Asp-125. In the substrate complex, loop L6 is in an open

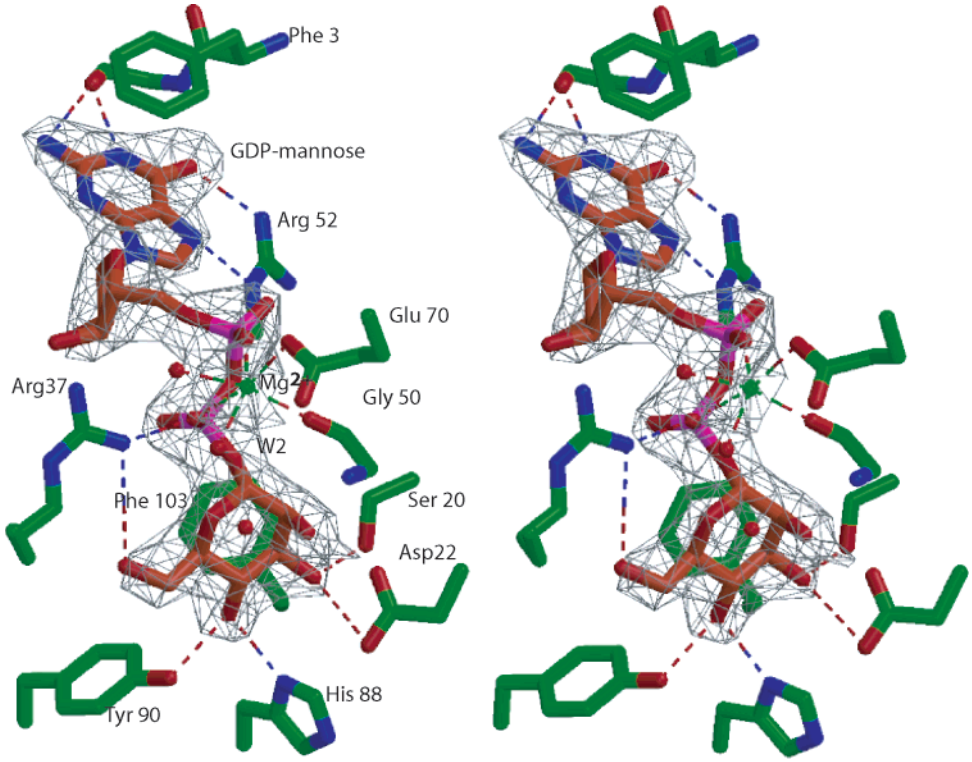

FIGURE 6: Stereoview of the active site of the Y103F mutant of GDPMH complexed with Mg^{2+} and GDP-α-D-mannose. Residues that interact with the substrate are indicated. The $2F_o - F_c$ electron density map corresponding to the substrate is shown (contour of 1σ). Phe-47, not shown for clarity, stacks over C6 of the mannose. Mg^{2+} is shown as a green sphere. Water molecules are shown as red spheres. W10 is above the mannosyl group.

conformation (Figure 7) with Gln-123 11.0 Å from the bound Mg^{2+} and His-124 18.4 Å from the divalent cation. In contrast, in the product complex, loop L6 is closed over the active site, permitting Gln-123 to directly coordinate to the Mg^{2+} (2.2 Å) and His-124 to reside in the second coordination sphere of the enzyme-bound Mg^{2+} (5.8 Å) (*7*), where it is well positioned to deprotonate the Mg^{2+}-bound water, W2 (Figure 7). This 9−12 Å movement of loop L6 opens and closes the active site, presumably to permit substrate recognition and binding. Clearly, in the open conformation, His-124 cannot function as a general base, nor can Gln-123 serve as a metal ligand. For these residues to function, loop L6 must close over the active site, as in the product complex. Additionally, the product complex differs from the substrate complex and the free enzyme in the main chain position of loop L2 (residues 37−43) (Figure 7).

Tyr-103 in the product complex donates a hydrogen bond to a β-phosphate oxygen atom of the GDP. This hydrogen bond, together with two hydrogen bonds from Arg-37, helps to stabilize the leaving group. The mutation of Tyr-103 to phenylalanine prevents formation of the hydrogen bond but maintains the aromatic contact with the mannose, analogous to that found between Tyr-103 and the Tris molecule in the product complex, even though the aromatic rings of Tyr-103 in the product complex and Phe-103 in the mutant−substrate complex are in slightly different positions. A comparison of both complexes suggests that the tyrosine OH group donates a hydrogen bond to the leaving glycosyl oxygen in the substrate complex. Accordingly, the Y103F mutation increases the K_m of GDP-α-D-mannose by 6.9-fold and decreases k_{cat} by 10^2-fold (Table 3). Residues Arg-37, Phe-47, and His-88 have different positions in the two structures. These movements, which are part of the changes in conformation of loop L2 (residues 37−43), are required to avoid a clash of the bulky C6-OH group of the substrate mannose with the guanidinium of Arg-37, which occupies an adjacent space in the product complex. The displacement of loop L2 by the C6-OH group of mannose is probably a consequence of this steric conflict.

Several water molecules present in the catalytic site are conserved with only small rearrangements between the two structures. Notably, water molecule W10, which in the product structure is close to the proposed position of C1 of the mannose, in the substrate structure is partially displaced by the presence of O2 of the mannose in such a way that it is now closer to C1 (3.5 Å). In this location, this water molecule is positioned well to be the entering nucleophile as suggested in one of the two proposed mechanisms (see below).

N-Linked β-Mannosyl Group. Surprisingly, in two of the three monomers in the asymmetric unit of the substrate complex, the X-ray structure showed the presence of a β-mannosyl group covalently bound, presumably N-linked, to the amide side chain of Asn-39. This mannose residue makes hydrogen bonds with the side chains of residues Arg-37, Arg-40, and Thr-38 and with the main chain NH group of Thr-38 (Figure 8). Because the mother liquor in which the crystals grew also contained glucose, it was possible that the hexose covalently bound to the protein was actually glucose, but there is no precedent for a direct glycosylation at a side chain amide. On the basis of this consideration, it was concluded that the residue was indeed a mannose in a β-linkage and that the reaction likely involved a glycosyl transfer from GDP-α-D-mannose with inversion.

The question of why this mannosylation is observed only in GDPMH containing the Y103F mutation remains. One

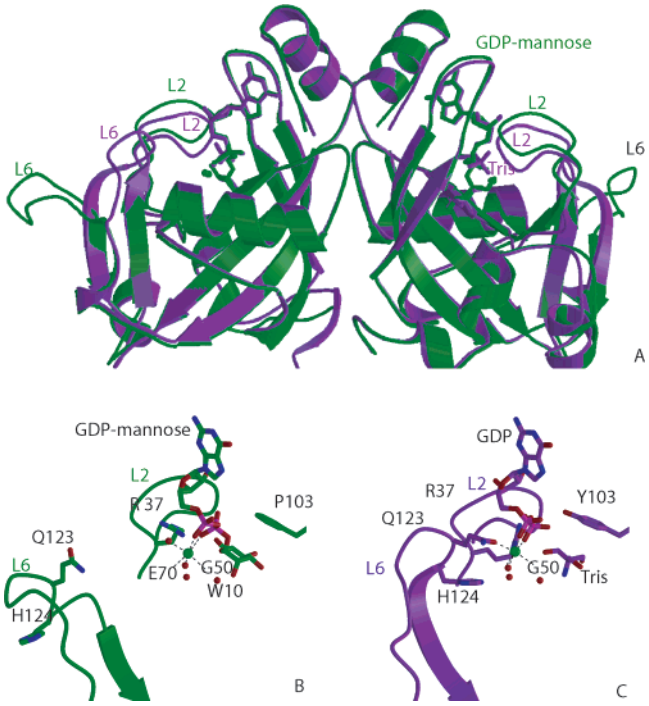

FIGURE 7: Comparison of the structures of the complexes of wild-type GDPMH with Mg^{2+} and GDP (purple) and the Y103F mutant with Mg^{2+} and GDP-mannose (green). (A) Overlap of the ribbon diagrams of the two structures. Bound substrate and product and displacement of loops L2 and L6 are shown. (B) Structure of the Y103F−Mg^{2+}−GDP-mannose (substrate) complex. In the structure, loop L6 is far from the active site (open conformation). (C) In the product complex, the (fortuitous) presence of a Tris molecule, which probably mimics the charge in the transition state, closes loop L6 carrying Gln-123, the metal ligand, and the His-124 catalytic base into their catalytically functional positions.

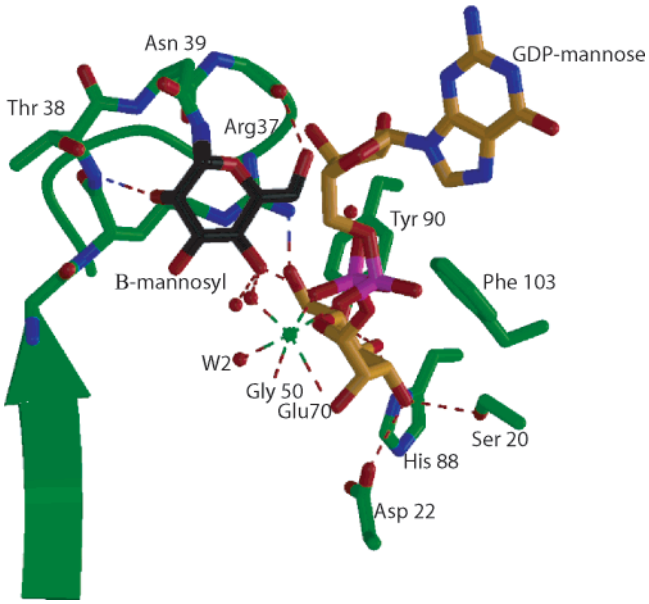

FIGURE 8: Position of the N-linked β-mannosyl group in the catalytic site of GDPMH. The structure is projected down the mannosyl C1−Asn-39 Nδ bond. The interactions of the mannose with other residues are indicated.

possibility is that as part of the hydrolytic reaction mechanism, mannose is first transferred to Asn-39 and the N−mannosyl bond is subsequently hydrolyzed in a manner that requires the OH group of Tyr-103. This explanation, however, is not compatible with the observation that the hydrolysis of GDP-mannose by GDPMH proceeds with inversion of configuration at C1 which requires a single transfer. A more likely possibility is that, given that hydrolysis of GDP-mannose by the Y103F mutant of GDPMH is a slow reaction, the residence time of the substrate in the enzyme is long, and on occasion, the oxocarbenium form of mannose alkylates a nearby residue, Asn-39. This side reaction may proceed by a mechanism similar to that proposed for other N-glycosyl transferases, aided by the coincidental proximity of Thr-38 and the main chain NH group of Arg-40, which may provide an "oxy-anion hole" similar to those present in authentic N-glycosyl transferases (*35*).[3] Searches by mass spectroscopy revealed no mannosylation by GDP-mannose in solution of wild-type GDPMH or of the R37Q/Y103F mutant. When present, this mannosylation of the Y103F mutant is not responsible for the opening of loop L6 in the crystal since the active site which is not mannosylated is also open.

Kinetic Effects of the Y103F and H124Q Single and Double Mutants. Because the Y103F mutation alters the position of His-124, moving its Nϵ approximately 12 Å farther from the metal-bound water (W2), the Y103F/H124Q double mutant was constructed to determine whether His-124 functioned as the general base, as in the wild-type enzyme (*2*). As summarized in Table 3, the H124Q single mutation was previously shown to decrease k_{cat} by $10^{3.4}$, equivalent to a 4.8 kcal/mol increase in the kinetic barrier to catalysis, to increase $K_m^{GDP-mannose}$ by a factor of 4.7, and to abolish the ascending limb of the k_{cat} versus pH−rate profile, replacing the pK_a of 6.70 with a weak, linear dependence of k_{cat} on $[OH^-]^{0.17}$ (*2*). Under the same conditions, the Y103F single mutation decreased k_{cat} $10^{2.0}$-fold (equivalent to 2.8 kcal/mol), increased $K_m^{GDP-mannose}$ 6.9-fold, and retained a pK_a of 6.56 in the k_{cat} versus pH−rate profile (Table 3).

Interestingly, the Y103F/H124Q double mutant decreased k_{cat} by only $10^{1.7}$-fold (2.4 kcal/mol), in comparison with that of the wild-type enzyme, increased $K_m^{GDP-mannose}$ by only 3.4-fold, and restored the pH dependence of k_{cat}, increasing the pK_a from 6.70 to 7.49 (Table 3). A separate kinetic assay of the double mutant (*11*) confirmed the formation of GDP as a product, indicating that the site of bond cleavage in GDP-α-D-mannose was unaltered from that found with the wild-type enzyme. Thus, adding the Y103F mutation to the kinetically more damaged H124Q mutant antagonistically restored k_{cat} in the double mutant to a value of $(7.0 \pm 0.3) \times 10^{-3}$ s^{-1}, comparable to that of the Y103F single mutant $[(3.2 \pm 0.3) \times 10^{-3}$ $s^{-1}]$. In the double mutant, the kinetic barrier to k_{cat} is only 2.4 kcal/mol relative to the wild type, departing from additivity by −5.2 kcal/mol. This departure from additivity, which provides a measure of the interaction energy between the two residues, likely results from the opposing structural effects of the two mutations (*36*). Conversely, adding the H124Q mutation had no further damaging effect on the Y103F mutant and may have slightly improved its catalytic properties (Table 3).

[3] The possibility that GDPMH catalyzes glycosyl transfers to other substrates is under investigation, but no glycosylation of seven monosaccharides was detected (*2*).

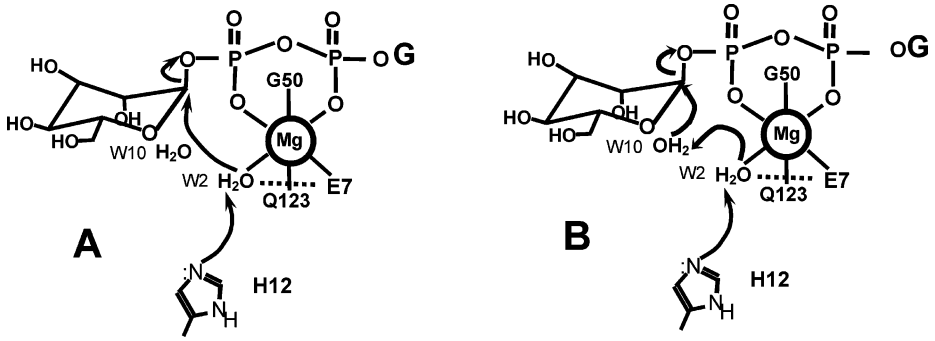

FIGURE 9: Alternative mechanisms of the GDPMH reaction. (A) Direct mechanism using the metal-bound hydroxyl (W2) as the entering nucleophile. (B) Mechanism using hydroxyl W2 as the base and W10 with the latter as the nucleophile.

In the H124Q mutant, Gln-124 may occlude access of external hydroxide to metal-bound water W2, decreasing the reaction rate by $10^{3.4}$ and essentially removing the dependence of the rate on OH^- concentration (*2*). The Y103F mutation changes the mechanism to one not requiring closing of the loop carrying the catalytic base and thus keeps Gln-124 out of the active site (Figure 7). This conformational change permits the direct participation of hydroxide from solvent in the deprotonation of the metal-bound water, W2, thereby increasing k_{cat} $10^{1.7}$-fold and restoring its pH dependence.

The small 2.2-fold increase in the k_{cat} of the Y103F mutant upon addition of the H124Q mutation is more difficult to explain since the mutated His-124 is far from the active site. It is noteworthy that, for an unknown reason, the pK_a of the metal-bound water in the Y103F/H124Q double mutant has increased by 0.93 unit, from 6.56 in Y103F to 7.49. Hence, the metal-bound hydroxide, which is fully formed at pH 9.3, is $10^{0.93}$-fold more nucleophilic in the double mutant than in the Y103F single mutant. A 2.2 (or $10^{0.34}$)-fold increase in k_{cat} resulting from a $10^{0.93}$-fold increase in nucleophilicity suggests a low β-nucleophile value of 0.37 (*37*), consistent with a mechanism with partially dissociative character, since a fully dissociative mechanism would have a β-nucleophile value of ~0.2 and an associative mechanism would have a value of ~0.8 (*37*). A dissociative mechanism was previously proposed on the basis of the extensive activation of the GDP leaving group by four catalytic residues and the essential Mg^{2+}, the important role of Asp-22 in stabilizing an incipient oxocarbenium ion at C1 of the mannose, and the low substrate activity of GDP-2F-α-D-mannose which would, by electron withdrawal, destabilize an oxocarbenium ion at C1 of the mannose (*1*).

The dependence of the kinetically determined pK_a in k_{cat} versus pH on the electrophilicity of the metal activator, as found with both wild-type GDPMH and the H124Q/Y103F/E70Q mutant (Table 4), establishes a central role of the metal-bound water molecule, W2, in the reaction mechanism. Since the pK_a of W2 is ≤6.7, possibly due to the proximity of His-124, W2 is largely deprotonated at physiological pH. Although W2 is too far from C1 in the structures of both complexes, it could, after a rearrangement of several groups, add directly to the incipient oxocarbenium transition state at C1 of the mannose (Figure 9A). More likely, this metal-bound hydroxide could deprotonate W10, which is better positioned to add to C1 of the mannose (Figure 9B). A third mechanism involving His-124, W5, and W10, proposed on the basis of favorable hydrogen bonding distances (*7*), may now be ruled out, since metal-bound water W2 was not proposed to participate in this process.

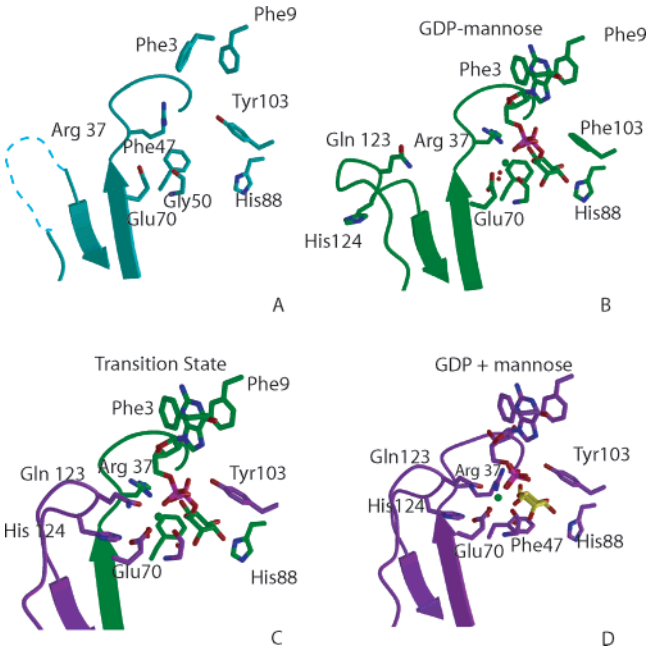

FIGURE 10: Snapshots of the catalytic cycle of GDPMH. (A) Crystallographic structure of the free enzyme. In this structure, loop L6 (dashed line) is disordered at the beginning of the cycle. (B) X-ray structure of the substrate complex. In this structure, although loop L6 becomes ordered, it remains in an open conformation. (C). Model of the GDPMH−transition state complex. This model was obtained by combining the coordinates of the enzyme in the product structure with the position of the GDP-mannose in the substrate structure (PDB entry 2GT4) distorting the mannose to a half-chair and elongating the mannosyl C1−GDP bond. In this model, loop L6 is in the closed conformation, bringing residues Gln-123 and His-124 into their active positions. This conformational change is probably triggered by the positive charge developed in the partially dissociative transition state acting on the negative charges in loop L6 (Asp-121, Glu-122, and Asp-125). (D) Product complex. This structure corresponds to the stage in the catalytic cycle before the release of products.

Mechanistic Implications of the Conformational Changes. The three structures of GDPMH, free enzyme, substrate complex, and product complex, suggest that major conformational changes take place during hydrolysis of GDP-mannose catalyzed by GDPMH (Figure 10). In the structure of the free enzyme, the loop spanning residues 119−125 is dynamically disordered (Figures 3 and 10A) as indicated by the lack of density in the X-ray structure and by the broadening of the imidazole ^{15}N resonances of His-124 in

the HMQC spectrum. After binding Mg^{2+} and GDP-mannose, the loop becomes ordered but in an open conformation in which the catalytic base, His-124, is more that 12 Å from the position required for catalysis (Figure 10B). This open conformation of the substrate complex appears to be incompatible with the catalytic requirements of the enzyme. In the structure of the product complex, on the other hand, the loop had closed onto the catalytic site, bringing His-124 into the position in which it can act as the catalytic base (closed conformation) (Figure 10D). One explanation of these observations might invoke the fact that the structure of the substrate complex was determined using the Y103F mutant of the enzyme. It is possible that the lack of the tyrosine OH group prevents the bound substrate from triggering the conformational change to that observed in the product complex. However, there is no direct involvement of the tyrosine OH group in stabilizing the closed conformation, nor are there other changes between the two structures that can explain why the conformational change does not take place in the substrate structure. A better explanation can be found if one takes into account the fact that the product structure contains a Tris molecule bound in the catalytic site, in the position occupied by the substrate mannose in the substrate complex. The hydroxyl groups of the Tris molecule make hydrogen bonds with side chains of the same residues that bind the mannose in the substrate structure. However, the Tris molecule has a positive charge not present in the substrate. The fact that this positively charged Tris molecule binds to the catalytic site is consistent with the proposed catalytic mechanism: a partially dissociative mechanism in which a positive charge develops on the mannose. If this is the case, it is possible that closing of the negatively charged catalytic loop L6 (which contains Asp-121, Glu-122, and Asp-125) takes place only as the positive charge is developing. In the Y103F mutant, the loop does not close because the hydroxyl of Tyr-103, which makes a hydrogen bond to the leaving oxygen atom of the β-phosphate, is probably required for the charge separation that takes place in the partially dissociative mechanism. The proposed transition state (Figure 10C), modeled by docking an oxocarbenium form of GDP-α-D-mannose into the closed, active conformation of the enzyme, fit well with no steric clashes.

As mentioned above, loop L2, which contains Arg-37, also has two different conformations, one in the free enzyme and the substrate complex and another in the product complex. In the product complex, the main chain of loop L2 is 1.2 Å closer to the position of the β-phosphate than in the substrate complex (Figure 10D). It appears that the interaction with GDP stabilizes Arg-37 in an inward position that pushes Phe-47 to a less favorable rotamer. This change in rotamer correlates with movements of Arg-37 and Pro-41. In its new position, Phe-47 forms a stacking interaction with C6 of the mannose.

The movement of loop L2, which places Arg-37 within hydrogen bonding distance of the β-phosphate, appears to be a consequence of the developing negative charge in the β-phosphate. Thus, it is tempting to suggest that loop L2 approaches the β-phosphate to neutralize the additional negative charge that is being developed as the phosphate separates from C1 of mannose. When the reaction is completed, Arg-37 neutralizes the additional full negative charge developed in the product. Accordingly, the R37Q mutation decreases k_{cat} 24-fold and increases the K_m of GDP-α-D-mannose 8.5-fold (Table 2) (*2*).

ACKNOWLEDGMENT

We are grateful to Dr. Ananya Majumdar for help with the NMR instrumentation. The X-ray data were collected at beamlines X6a and X25 of the National Synchrotron Light Source, Brookhaven National Laboratory.

SUPPORTING INFORMATION AVAILABLE

Four tables showing the number of shifted backbone resonances in various mutants (Table S1) and histidine imidazole chemical shifts at low and high pH of wild-type GDPMH (Table S2), the Y103F mutant (Table S3), and the Y103F/H124Q double mutant (Table S4). This material is available free of charge via the Internet at http://pubs.acs.org.

REFERENCES

1. Xia, Z., Azurmendi, H. F., Lairson, L. L., Withers, S. G., Gabelli, S. B., Bianchet, M. A., Amzel, L. M., and Mildvan, A. S. (2005) Mutational, structural, and kinetic evidence for a dissociative mechanism in the GDP-mannose mannosyl hydrolase reaction, *Biochemistry 44*, 8989−97.
2. Legler, P. M., Massiah, M. A., and Mildvan, A. S. (2002) Mutational, kinetic, and NMR studies of the mechanism of *E. coli* GDP-mannose mannosyl hydrolase, an unusual Nudix enzyme, *Biochemistry 41*, 10834−48.
3. Frick, D. N., Townsend, B. D., and Bessman, M. J. (1995) A novel GDP-mannose mannosyl hydrolase shares homology with the MutT family of enzymes, *J. Biol. Chem. 270*, 24086−91.
4. Legler, P. M., Massiah, M. A., Bessman, M. J., and Mildvan, A. S. (2000) GDP-mannose mannosyl hydrolase catalyzes nucleophilic substitution at carbon, unlike all other Nudix hydrolases, *Biochemistry 39*, 8603−8.
5. Bessman, M. J., Frick, D. N., and O'Handley, S. F. (1996) The MutT proteins or "Nudix" hydrolases, a family of versatile, widely distributed, "housecleaning" enzymes, *J. Biol. Chem. 271*, 25059−62.
6. Harris, T. K., Wu, G., Massiah, M. A., and Mildvan, A. S. (2000) Mutational, kinetic, and NMR studies of the roles of conserved glutamate residues and of lysine-39 in the mechanism of the MutT pyrophosphohydrolase, *Biochemistry 39*, 1655−74.
7. Gabelli, S. B., Bianchet, M. A., Azurmendi, H. F., Xia, Z., Saraswat, V., Mildvan, A. S., and Amzel, L. M. (2004) Structure and mechanism of GDP-mannose glycosyl hydrolase, a Nudix enzyme that cleaves at carbon instead of phosphorus, *Structure 12*, 927−35.
8. Mildvan, A. S., Xia, Z., Azurmendi, H. F., Saraswat, V., Legler, P. M., Massiah, M. A., Gabelli, S. B., Bianchet, M. A., Kang, L. W., and Amzel, L. M. (2005) Structures and mechanisms of Nudix hydrolases, *Arch. Biochem. Biophys. 433*, 129−43.
9. Withers, S. G. (2001) Mechanism of glycosyl transferases and hydrolases, *Carbohydr. Polym. 44*, 325−37.
10. Gabelli, S. B., Bianchet, M. A., Bessman, M. J., and Amzel, L. M. (2001) The structure of ADP-ribose pyrophosphatase reveals the structural basis for the versatility of the Nudix family, *Nat. Struct. Biol. 8*, 467−72.
11. Bücher, T., and Pfleiderer, G. (1955) Pyruvate kinase from rabbit muscle, *Methods Enzymol. 1*, 435−40.
12. Legler, P. M., Lee, H. C., Peisach, J., and Mildvan, A. S. (2002) Kinetic and magnetic resonance studies of the role of metal ions in the mechanism of *Escherichia coli* GDP-mannose mannosyl hydrolase, an unusual nudix enzyme, *Biochemistry 41*, 4655−68.
13. Gill, S. C., and von Hippel, P. H. (1989) Calculation of protein extinction coefficients from amino acid sequence data, *Anal. Biochem. 182*, 319−26.
14. Mahuren, J. D., Coburn, S. P., Slominski, A., and Wortsman, J. (2001) Microassay of phosphate provides a general method for measuring the activity of phosphatases using physiological non-chromogenic substrates such as lysophosphatidic acid, *Anal. Biochem. 298*, 241−5.

15. Czerwinski, R. M., Johnson, W. H. J., Whitman, C. P., Harris, T. K., Abeygunawardana, C., and Mildvan, A. S. (1997) Kinetic and structural effects of mutations of the catalytic amino-terminal proline in 4-oxalocrotonate tautomerase, *Biochemistry 36*, 14551−60.
16. Otwinowski, Z., and Minor, W. (1997) Processing of X-ray diffraction data collected in oscillation mode, *Methods Enzymol. 277*, 307−26.
17. Navaza, J. (1994) AMoRe: An automated package for molecular replacement, *Acta Crystallogr. A50*, 157−63.
18. Collaborative Computational Project Number 4 (1994) The CCP4 Suite: Programs for Protein Crystallography, *Acta Crystallogr. D50*, 760−3.
19. Jones, T. A., Zou, J. Y., Cowan, S. W., and Kjelgaard, M. (1991) Improved methods for binding protein models to electron density maps and the location of errors in these models, *Acta Crystallogr. A42*, 110−9.
20. Perrakis, A., Harkiolaki, M., Wilson, K. S., and Lamzin, V. S. (2001) ARP/wARP and molecular replacement, *Acta Crystallogr. D57*, 1445−50.
21. Laskowski, R., MacArthur, M., Moss, D., and Thornton, J. (1993) PROCHECK: A program to check the sterochemical quality of protein structures, *J. Appl. Crystallogr. 26*, 283−91.
22. Kleywegt, G. J., and Jones, T. A. (1994) in *Halloween...Masks and Bones* (Bailey, S., Hubbard, R., and Waller, D., Eds.) pp 59−66, SERC, Warrington, U.K.
23. Kraulis, J. (1991) MOLSCRIPT: A program to produce both detailed and schematic plots of protein structure, *J. Appl. Crystallogr. 24*, 946−50.
24. Esnouf, R. M. (1999) Further additions to Molscript version 1.4, including reading and countouring of electron density maps, *Acta Crystallogr. D55*, 938−40.
25. DeLano, W. L. (2002) *The PyMOL Molecular Graphics System*, DeLano Scientific, San Carlos, CA.
26. Pelton, J. G., Torchia, D. A., Meadow, N. D., and Roseman, S. (1993) Tautomeric states of the active-sites histidines of phosphorylated and un phosphorylated IIIGlc, a signal-transducing protein from *Escherichia coli*, using two-dimensional heteronuclear NMR techniques, *Protein Sci. 2*, 543−58.
27. Delaglio, F., Grzesiek, S., Vuister, G. W., Zhu, G., Pfeifer, J., and Bax, A. (1995) NMRPipe: A multidimensional spectral processing system based on UNIX pipes, *J. Biomol. NMR 6*, 277−93.
28. Goddard, T. D., and Kneller, D. G. (2004) *Sparky 3*, University of California, San Francisco.
29. Bachovchin, W. W. (1986) ^{15}N NMR spectroscopy of hydrogen-bonding interactions in the active site of serine proteases: Evidence for a moving histidine mechanism, *Biochemistry 25*, 7751−9.
30. Jardetzky, O., and Roberts, G. C. K. (1981) in *NMR in Molecular Biology*, pp 115−42, Academic Press, New York.
31. Dixon, M., and Webb, E. C. (1997) in *Enzymes*, 3rd ed., p 163, Academic Press, New York.
32. Gupta, R. K., Oesterling, R. M., and Mildvan, A. S. (1976) Dual divalent cation requirement for the activation of pyruvate kinase: Essential roles of both enzyme- and nucleotide-bound divalent cations, *Biochemistry 15*, 2881−7.
33. Bruice, P. Y. (2004) in *Organic Chemistry*, 4th ed., p 1008, Prentice Hall, Upper Saddle River, NJ.
34. Huang, Y. C., Grodsky, N. B., Kim, T.-K., and Colman, R. F. (2004) Ligands of the Mn^{2+} bound to porcine mitochondrial NADP-dependent isocitrate dehydrogenase, as assessed by mutgenesis, *Biochemistry 43*, 2821−8.
35. Imperiali, B., O'Connor, S. E., Hendrickson, T., and Kellenberger, C. (1999) Chemistry and biology of asparagine-linked glycosylation, *Pure Appl. Chem. 71*, 777−87.
36. Mildvan, A. S., Weber, D. J., and Kuliopulos, A. (1992) Quantitative Interpretations of Double Mutations of Enzymes, *Arch. Biochem. Biophys. 294*, 327−40.
37. Jencks, W. P. (1969) in *Catalysis in Chemistry and Enzymology*, p 81, McGraw-Hill, New York.

BI061239G